Available online at www.sciencedirect.com
ScienceDirect
International Journal of Heat and Mass Transfer 50 (2007) 5194–5203
International Journal of HEAT and MASS TRANSFER
www.elsevier.com/locate/ijhmt

Heat transfer and pressure drop during HFC refrigerant vaporisation inside a brazed plate heat exchanger

G.A. Longo *, A. Gasparella

University of Padova, Department of Management and Engineering, Stradella S. Nicola 3, I-36100 Vicenza, Italy

Received 6 November 2006; received in revised form 30 June 2007
Available online 14 August 2007

Abstract

This paper presents the experimental heat transfer coefficients and pressure drop measured during HFC refrigerant 134a, 410A and 236fa vaporisation inside a small brazed plate heat exchanger: the effects of heat flux, refrigerant mass flux, saturation temperature, outlet conditions and fluid properties are investigated. The experimental results are reported in terms of refrigerant side heat transfer coefficients and frictional pressure drop. The heat transfer coefficients show great sensitivity to heat flux and outlet conditions and weak sensitivity to saturation temperature. The frictional pressure drop shows a linear dependence on the kinetic energy per unit volume of the refrigerant flow. HFC-410A shows heat transfer coefficients 40–50% higher than HFC-134a and 50–60% higher than HFC-236fa and frictional pressure drops 40–50% lower than HFC-134a and 50–60% lower than HFC-236fa. The experimental heat transfer coefficients are compared with two well-known equations for nucleate boiling [M.G. Cooper, Heat flows rates in saturated pool boiling – a wide ranging examination using reduced properties, Advanced Heat Transfer, Academic Press, Orlando, Florida, 1984, pp. 157–239; D. Gorenflo, Pool boiling, in: E.U. Schlünder (Ed.), VDI Heat Atlas, Dusseldorf, Germany, 1993, Ha1-25] and a correlation for frictional pressure drop is proposed.

1. Introduction

In the 1990s hydrofluorocarbon (HFC) refrigerants have been commercialised to substitute traditional chlorofluorocarbon (CFC) and hydrochlorofluorocarbon (HCFC) refrigerants subject to phase out for their high ozone depletion potential.

HFC-134a is the world-wide choice to replace CFC-12 in domestic refrigeration and mobile air conditioning, whereas HFC-407C and HFC-410A are the alternative for HCFC-22 in chillers and heat pumps. HFC-407C, a non azeotropic ternary mixture HFC-32/HFC-125/HFC-134a (23/25/52 wt%), is the equivalent pressure replacement which can be used also in existing equipment. HFC-410A, a nearly azeotropic mixture HFC-32/HFC-125 (50/50% wt%), is the alternative for use in new equipment specifically designed for its high operating pressure. More recently HFC-236fa, a low pressure refrigerant, has been proposed as substitute for CFC-114 in heat pump application and in submarine air conditioning systems.

Traditional plate heat exchangers with gaskets (PHE) have been successfully used since the 1930s for single-phase heat transfer from liquid-to-liquid in chemical and food processing industries. In the late seventies a new type of PHE, the brazed plate heat exchangers (BPHE), has been developed for two-phase heat transfer, particularly as evaporators and condensers in chillers and heat pumps.

In open literature, it is possible to find several works on traditional PHE in single-phase liquid-to-liquid heat transfer, whereas limited data can be found on HFC refrigerant vaporisation and condensation inside BPHE. Yan and Lin [1] and Yan et al. [2] experimentally investigated the effects of mean vapour quality, mass flux, heat flux and saturation pressure on heat transfer and pressure drop during HFC-134a vaporisation and condensation inside a BPHE. They also presented empirical correlations for heat transfer

* Corresponding author. Tel.: +39 0444 998726; fax: +39 0444 998888.
E-mail address: tony@gest.unipd.it (G.A. Longo).

0017-9310/$ - see front matter © 2007 Elsevier Ltd. All rights reserved.
doi:10.1016/j.ijheatmasstransfer.2007.07.001

Nomenclature

A	nominal area of a plate, m^2
b	height of the corrugation, m
Bo	boiling number, $q/G\Delta J_{LG}$
c_p	specific heat capacity, J kg^{-1} K^{-1}
c_{Ra}	correction term in Eq. (26)
d_h	hydraulic diameter, $d_h = 2$ b, m
F	correction term in Eq. (26)
g	gravity acceleration, m s^{-2}
G	mass flux, $G = m/(n_{ch}Wb)$, kg m^{-2} s^{-1}
h	heat transfer coefficient, W m^{-2} K^{-1}
J	specific enthalpy, J kg^{-1}
KE/V	kinetic energy per unit volume, J m^{-3}
L	flow length of the plate, m
m	mass flow rate, kg s^{-1}
M	molecular weight, kg $kmol^{-1}$
n_{ch}	number of channels
N	number of effective plates
p	pressure, Pa
P	corrugation pitch, m
Pr	Prandtl number, $Pr = \mu c_p/\lambda$
q	heat flux, $q = Q/S$, W m^{-2}
Q	heat flow rate, W
R_a	arithmetic mean roughness (ISO 4271/1), μm
R_p	roughness (DIN 4762/1), μm
S	nominal heat transfer area, m^2
s	plate wall thickness, m
T	temperature, K
U	overall heat transfer coefficient, W m^{-2} K^{-1}
v	specific volume, m^3 kg^{-1}
V	volume, m^3
W	width of the plate, m
X	vapour quality, $X = (J - J_L)/\Delta J_{LG}$
XX	co-ordinate in Fig. 3 (Eq. (12))
X_{tt}	Martinelli parameter (Eq. (34))
YY	co-ordinate in Fig. 3 (Eq. (13))

Greek symbols

β	inclination angle of the corrugation
δ	difference
ΔJ_{LG}	latent heat of vaporisation, J kg^{-1}
λ	thermal conductivity, W m^{-1} K^{-1}
μ	viscosity, kg m^{-1} s^{-1}
ρ	density, kg m^{-3}

Subscripts

a	momentum
boil	boiling
c	manifold and port
E	external channels
eq	equivalent
f	frictional
g	gravity
G	vapour phase
I	internal channels
in	inlet
L	liquid phase
LG	liquid gas phase change
ln	logarithmic
m	average value
out	outlet
p	plate
pb	pre-evaporator
r	refrigerant
t	total
sat	saturation
sup	super-heating
w	water
wi	water inlet
wo	water outlet
0	reference conditions in Eq. (26)

coefficient and friction factor based on their experimental data. Hsieh and Lin [3,4] reported experimental data on vaporisation heat transfer and pressure drop of HFC-410A in a BPHE. The effects of mean vapour quality, mass flux, heat flux and saturation pressure were evaluated and empirical correlations were proposed for heat transfer coefficient and friction factor. Han et al. [5] presented experimental heat transfer coefficients and pressure drop measured during HFC-410A vaporisation inside a BPHE. The effects of mass flux, heat flux, saturation temperature and plate geometry (inclination angle of the corrugation) were evaluated and empirical correlations were proposed for Nusselt number and friction factor. Jokar et al. [6,7] reported experimental data on HFC-134a condensation and vaporisation inside BPHE and proposed empirical correlations for heat transfer and pressure drop. Kuo et al. [8] reported experimental data on HFC-410A condensation inside a PHE and proposed empirical correlations for heat transfer and pressure drop. Jassim et al. [9,10] analysed the pressure drop and the flow regime in adiabatic two-phase flow of HFC-134a through a PHE with herringbone and bumpy corrugation: a two-phase pressure drop model and a flow regime map were proposed.

This paper presents the experimental heat transfer coefficients and pressure drop measured during HFC refrigerants 236fa, 134 and 410A vaporisation inside a small commercial BPHE: the effects of heat flux, refrigerant mass flux, saturation temperature, outlet conditions and fluids properties are investigated.

2. Experimental set-up and procedures

The experimental facility, shown in Fig. 1, consists of a refrigerant loop, a water–glycol loop and a refrigerated

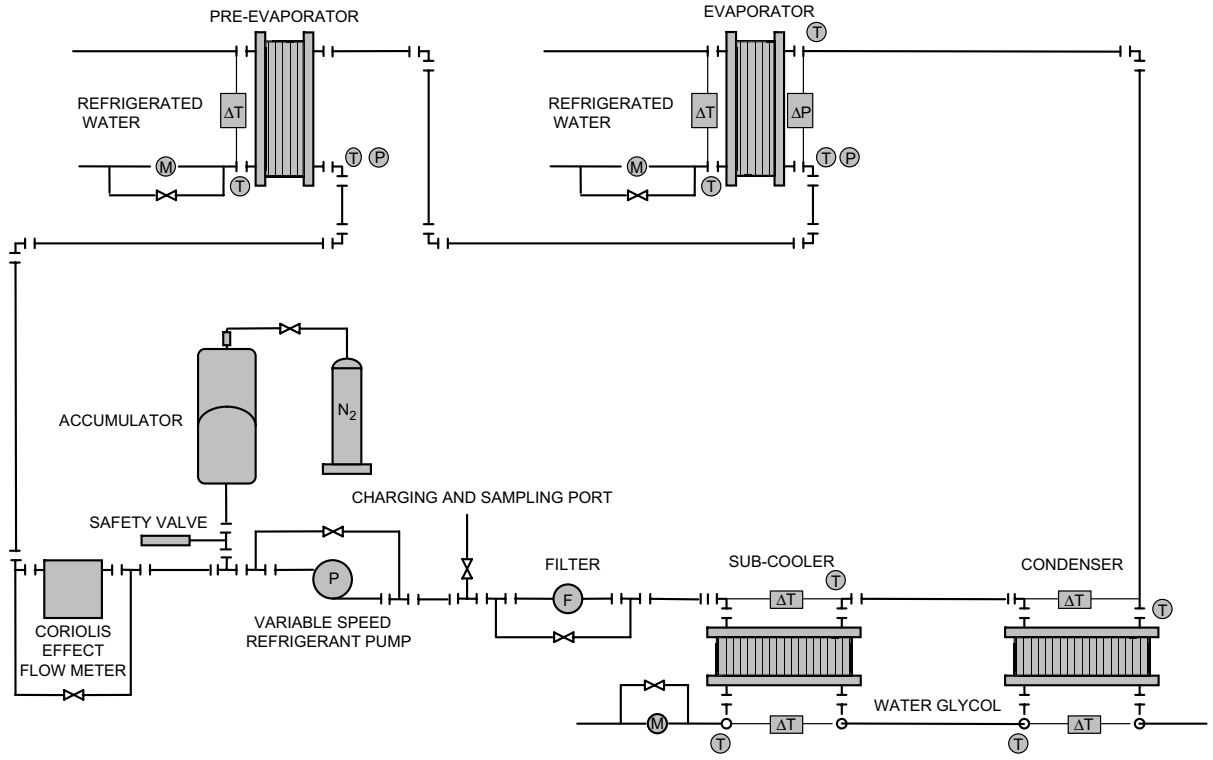

Fig. 1. Schematic view of the experimental test rig.

water loop. In the first loop the refrigerant is pumped from the sub-cooler into the pre-evaporator where it is partially evaporated to achieve the set quality at the evaporator inlet. The refrigerant goes through the evaporator where it is evaporated and eventually super-heated and then it comes back to the condenser and the sub-cooler. A variable speed volumetric pump varies the refrigerant flow rate, whereas a bladder accumulator connected to a nitrogen bottle and a pressure regulator controls the operating pressure in the refrigerant loop. The second loop is able to supply a water–glycol flow at a constant temperature in the range of −10 to 30 °C with a stability within ±0.1 K used to feed the sub-cooler and the condenser, whereas the third loop supplies a refrigerated water flow at a constant temperature in the range of 3–30 °C with a stability within ±0.1 K used to feed the evaporator and the pre-evaporator. The evaporator is a BPHE consisting of 10 plates, 72 mm in width and 310 mm in length, which present a macro-scale herringbone corrugation with an inclination angle of 65° and a corrugation amplitude of 2 mm. Fig. 2 and Table 1 give the main geometrical characteristics of the BPHE tested. The temperatures of refrigerant and water at the inlet and outlet of the evaporator and the pre-evaporator are measured by T-type thermocouples (uncertainty (95% CL) within ±0.1 K), whereas water temperature drops through the evaporator and the pre-evaporator are measured by T-type thermopiles (uncertainty (95% CL) within ±0.05 K). The refrigerant pressures at the inlet of the evaporator and the pre-evaporator are measured by two absolute strain-gage pressure transducers

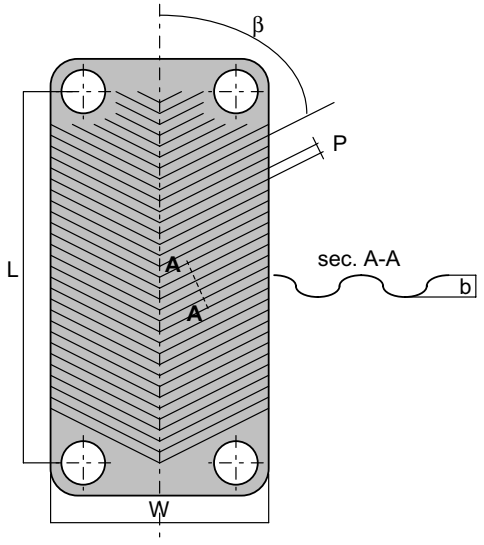

Fig. 2. Schematic view of the plate.

(uncertainty (95% CL) within 0.075% f.s.), whereas the refrigerant pressure drop through the evaporator is measured by a strain-gage differential pressure transducer (uncertainty (95% CL) within 0.075% f.s.). The refrigerant mass flow rate is measured by means of a Coriolis effect mass flow meter (uncertainty (95% CL) of 0.1% of the measured value), whereas the water flow rates through the evaporator and the pre-evaporator are measured by means of magnetic flow meters (uncertainty (95% CL) of 0.15% of

Table 1
Geometrical characteristics

Fluid flow plate length L (mm)	278.0
Plate width W (mm)	72.0
Area of the plate A (m^2)	0.020
Corrugation type	Herringbone
Angle of the corrugation β (°)	65
Corrugation amplitude b (mm)	2.0
Corrugation pitch P (mm)	8.0
Plate roughness R_a (μm)	0.4
Plate roughness R_p (μm)	1.0
Number of plates	10
Channels on refrigerant side	4
Channels on water side	5

Table 2
Specification of the different measuring devices

Devices	Type	Uncertainty (95% CL)	Range
Thermometers	T-type thermocouples	0.1 K	−20 to 80 °C
Differential thermometers	T-type thermopiles	0.05 K	−20 to 80 °C
Abs. pressure transducers	Strain-gage	0.075% f.s.	0 to 2.0 MPa
Diff. pressure transducers	Strain-gage	0.075% f.s.	0 to 0.3 MPa
Refrigerant flow meters	Coriolis effect	0.1%	0 to 300 kg/h
Water flow meters	Magnetic	0.15%	100 to 1200 l/h

the f.s.). All the measurements are scanned and recorded by a data logger linked to a PC. Table 2 gives the main features of the different measuring devices in the experimental rig. Prior to the start of each test the refrigerant is re-circulated through the circuit, the condenser and the sub-cooler are fed with water glycol at a constant temperature and the evaporator and pre-evaporator are fed with water at a constant temperature. The refrigerant pressure and vapour quality at the inlet of the evaporator and the vapour quality or super-heating at the outlet of the evaporator are controlled by adjusting the bladder accumulator, the volumetric pump, the flow rate and the temperature of the water glycol and the refrigerated water. Once temperature, pressure, flow rate and vapour quality steady state conditions are achieved at the evaporator inlet and outlet both on refrigerant and water sides all the readings are recorded for a set time and the average value during this time is computed for each parameter collected. The experimental results are reported in terms of refrigerant side heat transfer coefficients and frictional pressure drop.

3. Data reduction

The overall heat transfer coefficient in the evaporator U is equal to the ratio between the heat flow rate Q, the nominal heat transfer area S and the logarithmic mean temperature difference ΔT_{ln}.

$$U = Q/(S\Delta T_{ln}) \tag{1}$$

The heat flow rate is derived from a thermal balance on the water side of the evaporator:

$$Q = m_w c_{pw} |\Delta T_w| \tag{2}$$

where m_w is the water flow rate, c_{pw} the water specific heat capacity and $|\Delta T_w|$ the absolute value of the temperature variation on the water side of the evaporator. The nominal heat transfer area of the evaporator

$$S = NA \tag{3}$$

is equal to the nominal projected area $A = L \times W$ of the single plate multiplied by the number N of the effective elements in heat transfer, as suggested by Shah and Focke [11].

When the evaporator works only in two-phase heat transfer the logarithmic mean temperature difference is equal to

$$\Delta T_{ln} = (T_{wi} - T_{wo})/\ln[(T_{wi} - T_{sat})/(T_{wo} - T_{sat})] \tag{4}$$

where T_{sat} is the average saturation temperature (dew point) of the refrigerant derived from the average pressure measured on refrigerant side and T_{wi} and T_{wo} the water temperatures at the inlet and the outlet of the evaporator.

Claesson [12] shows that, although the boiling heat transfer coefficient and the overall heat transfer coefficient are not constant inside a BPHE evaporator, the logarithmic mean temperature difference approach may be used if the boiling heat transfer is governed by heat flux and the logarithmic mean temperature difference is not too small (>4–5 °C).

When the evaporator works both in vaporisation and super-heating, Dutto et al. [13] and Fernando et al. [14] suggested the following expression for the logarithmic mean temperature difference:

$$\Delta T_{ln} = Q/[(Q_{boil}/\Delta T_{ln.boil}) + (Q_{sup}/\Delta T_{ln.sup})] \tag{5}$$

where

$$Q_{boil} = m_w c_{pw}(T_{wm} - T_{wo}) \tag{6}$$

$$Q_{sup} = m_w c_{pw}(T_{wi} - T_{wm}) \tag{7}$$

are the heat flow rate exchanged in the boiling and super-heating zones,

$$\Delta T_{ln.boil} = (T_{wm} - T_{wo})/\ln[(T_{wm} - T_{sat})/(T_{wo} - T_{sat})] \tag{8}$$

$$\Delta T_{ln.sup} = [(T_{wi} - T_{rout}) - (T_{wm} - T_{sat})]/\ln[(T_{wi} - T_{rout})/(T_{wm} - T_{sat})] \tag{9}$$

are the logarithmic mean temperature difference in the boiling and super-heating zones, whereas T_{wm} is the water temperature between the super-heating and the boiling zone and T_{rout} is the refrigerant temperature at the outlet of the evaporator. The water temperature between the super-heating and the boiling zone is calculated from

$$T_{wm} = T_{wi} - m_r c_{pGr}(T_{rout} - T_{sat})/(m_w c_{pw}) \tag{10}$$

where m_r is the refrigerant flow rate and c_{pGr} is the specific heat capacity of the refrigerant vapour.

This approach computes the overall heat transfer coefficient of the whole evaporator U as the average value between the overall heat transfer coefficient of the boiling zone U_{boil} and that of the super-heating zone U_{sup} weighted on the basis of the respective heat transfer area. In this way it is possible to directly compare the heat transfer performance of an evaporator working only in two-phase heat transfer with that of an evaporator working also in vapour super-heating.

The average heat transfer coefficient on the refrigerant side of the evaporator h_r is derived from the global heat transfer coefficient U assuming no fouling resistances

$$h_r = (1/U - s/\lambda_p - 1/h_w)^{-1} \tag{11}$$

by computing the water side heat transfer coefficient h_w using a modified Wilson plot technique. A specific set of experimental water-to-water tests was carried out on the evaporator to determine the calibration correlation for heat transfer on the water side, in accordance with Muley and Manglick [15]. This modification of the classical Wilson plot technique incorporates an account of variable fluid property effects: Fig. 3 shows the water-to-water data plotted on the co-ordinates

$$XX = (\lambda_I/\lambda_E)(Re_I/Re_E)^{0.766}(Pr_I/Pr_E)^{0.333} \tag{12}$$

$$YY = (1/U - s/\lambda_p)[(\lambda_I/d_h)Re_I^{0.766}Pr_I^{0.333}] \tag{13}$$

where subscripts I and E refer to the internal channels (normally refrigerant side) and to the external channels (normally water side) of the evaporator, respectively. The slope of the plot gives the constant in the calibration correlation, a power-law type, for heat transfer coefficients on the water side. The exponent on Reynolds number $n = 0.766$ results from a best fitting procedure on the experimental data. The calibration correlation for water side heat transfer coefficient results

$$h_w = 0.277(\lambda_w/d_h)Re_w^{0.766}Pr_w^{0.333} \tag{14}$$
$$5 < Pr_w < 10 \quad 200 < Re_w < 1200$$

It should be noted that Eq. (14) is only a calibration correlation for present test facility, valid only over the limited range of present water-to-water data.

The refrigerant vapour quality at the evaporator inlet and outlet X_{in} and X_{out} are computed starting from the refrigerant temperature $T_{pb.in}$ and pressure $p_{pb.in}$ at the inlet of the pre-evaporator (sub-cooled liquid condition) considering the heat flow rate exchanged in the pre-evaporator and in the evaporator Q_{pb} and Q and the pressure at the inlet and outlet p_{in} and p_{out} of the evaporator as follows:

$$X_{in} = f(J_{in}, p_{in}) \tag{15}$$

$$X_{out} = f(J_{out}, p_{out}) \tag{16}$$

$$J_{in} = J_{pb.in}(T_{pb.in}, p_{pb.in}) + Q_{pb}/m_r \tag{17}$$

$$J_{out} = J_{in} + Q/m_r \tag{18}$$

$$Q_{pb} = m_{pb.w}c_{pw}|\Delta T_{pb.w}| \tag{19}$$

where J is the specific enthalpy of the refrigerant, m_r the refrigerant mass flow rate, $m_{pb.w}$ the water flow rate and $|\Delta T_{pb.w}|$ the absolute value of the temperature variation on the water side of the pre-evaporator.

The frictional pressure drop on refrigerant side Δp_f is computed by subtracting the momentum pressure drop Δp_a, the gravity pressure drop Δp_g and the manifolds and ports pressure drops Δp_c from the total pressure drop measured Δp_t

$$\Delta p_f = \Delta p_t - \Delta p_a - \Delta p_g - \Delta p_c \tag{20}$$

The momentum and gravity pressure drops are estimated by the homogeneous model for two-phase flow as follows:

$$\Delta p_a = G^2(v_G - v_L)\Delta X \tag{21}$$

$$\Delta p_g = g\rho_m L \tag{22}$$

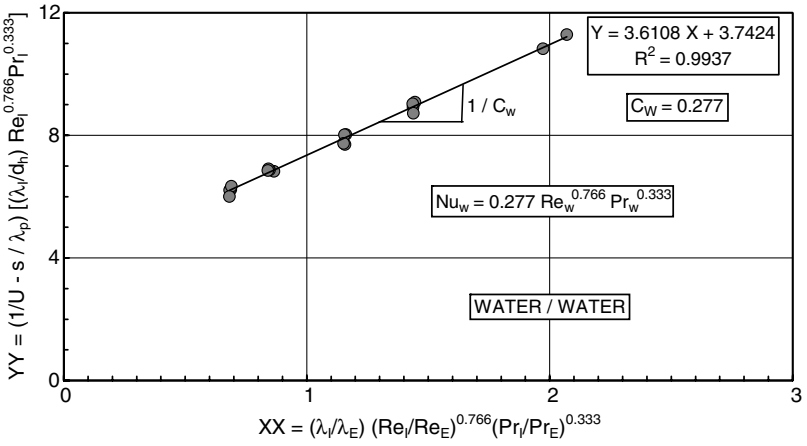

Fig. 3. Modified Wilson plot results for calibration of water side heat transfer coefficient.

where v_L and v_G are the specific volume of liquid and vapour phase, ΔX is the vapour quality change between inlet and outlet,

$$\rho_m = [X_m/\rho_G + (1 - X_m)/\rho_L]^{-1} \quad (23)$$

is the average two-phase density between inlet and outlet calculated by the homogeneous model and X_m in the average vapour quality between inlet and outlet.

The pressure drops in the inlet and outlet manifolds and ports are empirically estimated, in accordance with Shah and Focke [11], as follows:

$$\Delta p_c = 1.5G^2/(2\rho_m) \quad (24)$$

The refrigerant properties are evaluated by Refprop 7.0 [16].

4. Analysis of the results

Three different sets of vaporisation tests with refrigerant up-flow and water down-flow are carried out at three different saturation temperatures (10, 15 and 20 °C) and four different evaporator outlet conditions (vapour quality around 0.80 and 1.00, vapour super-heating around 5 and 10 °C), whereas the inlet vapour quality ranges between 0.2 and 0.4. Therefore, for each outlet condition tested, there is a direct connection between heat flux and mass flux and it is difficult to separate the two contributions.

The first set includes 80 tests with HFC-134a, the second 68 tests with HFC-410A, the third 57 tests with HFC-236fa. Table 3 gives the main operating conditions in the evaporator under experimental tests: refrigerant saturation temperature T_{sat} and pressure p_{sat}, inlet and outlet refrigerant vapour quality X_{in} and X_{out}, outlet refrigerant super-heating ΔT_{sup}, mass flux on refrigerant side G_r and water side G_w, heat flux q. The operating conditions investigated are typical for the evaporator of vapour compression chillers and heat pumps in air conditioning application.

A detailed error analysis performed in accordance with Kline and McClintock [17] indicates an overall uncertainty within ±12% for the refrigerant heat transfer coefficient measurement and within ±7% for the refrigerant pressure drop measurement.

Figs. 4–6 show the average heat transfer coefficients on the refrigerant side against heat flux for three different saturation temperatures (10, 15 and 20 °C) and four different evaporator outlet conditions (vapour quality around 0.80 and 1.00, vapour super-heating around 5 and 10 °C) for refrigerant HFC-236fa, HFC-134a and HFC-410A, respectively.

The heat transfer coefficients show great sensitivity to heat flux and outlet condition and weak sensitivity to saturation temperature for all the refrigerants tested. The saturated boiling heat transfer coefficients with an outlet vapour quality around 0.80 are from 2 to 10% higher than the saturated boiling heat transfer coefficients with an outlet vapour quality around 1.00, 5–20% higher than the heat transfer coefficients with 5 °C of outlet vapour super-heating and 30–40% higher than the heat transfer coefficients with 10 °C of outlet vapour super-heating. The weak decrease of the heat transfer coefficient with increasing vapour quality is probably due to dryout inception in the upper part of the evaporator. The marked decrease of the heat transfer coefficient with vapour super-heating is due to the increase in the super-heating portion of the heat transfer surface which is affected by gas single phase heat transfer coefficients one or two orders of magnitude lower than the two phase heat transfer coefficients in the boiling portion of the heat transfer surface. These experimental results are in fair agreement with those obtained by Claesson and Palm [18] on HCFC-22 vaporisation inside a small BPHE.

The correlation between the saturated boiling heat transfer coefficients ($X_{out} \leqslant 1$) and heat flux is well represented by a power-law function with an exponent between 0.4 and 0.6. It should be noted that, as already stated, it is difficult to separate the contributions of heat flux and mass flux as the different sets of experimental tests are carried out with an almost constant vapour quality change through the evaporator.

HFC-410A shows heat transfer coefficients 40–50% higher than HFC-134a and 50–60% higher than HFC-236fa under the same operating conditions.

The saturated boiling experimental heat transfer coefficients ($X_{out} \leqslant 1$) are compared with two well-known correlations for nucleate boiling: Cooper [19] and Gorenflo [20] equations.

The Cooper [19] equation, developed for nucleate pool boiling, accounts for heat flux, surface roughness and reduced pressure effects as follows:

$$h_r = 55p^{*(0.12-0.2\log_{10}Rp)}(-\log_{10}p^*)^{-0.55}q^{0.67}M^{-0.5} \quad (25)$$

where $p^* = p/p_{cr}$ is the reduced pressure, R_p (μm) the roughness as defined in German standard DIN 4762/1, q (W/m^2) the heat flux and M the molecular weight of the fluid. In the present analysis the heat transfer coefficient and heat flux are referred to the nominal heat

Table 3
Operating conditions during experimental tests

Fluid	Runs	T_{sat} (°C)	p_{sat} (MPa)	X_{in}	X_{out}	ΔT_{sup} (°C)	G_r (kg/m^2 s)	G_w (kg/m^2 s)	q (kW/m^2)
HFC-134a	80	9.7–20.3	0.41–0.57	0.16–0.39	0.78–1.00	3.7–11.4	11.8–36.7	42.4–231.5	4.5–19.7
HFC-410A	64	9.8–20.3	1.08–1.46	0.20–0.35	0.79–1.00	5.2–10.6	15.5–40.1	53.4–190.5	5.9–26.1
HFC-236fa	57	9.9–20.3	0.16–0.20	0.17–0.39	0.79–1.00	5.1–10.6	11.4–27.6	30.5–158.7	3.1–13.9

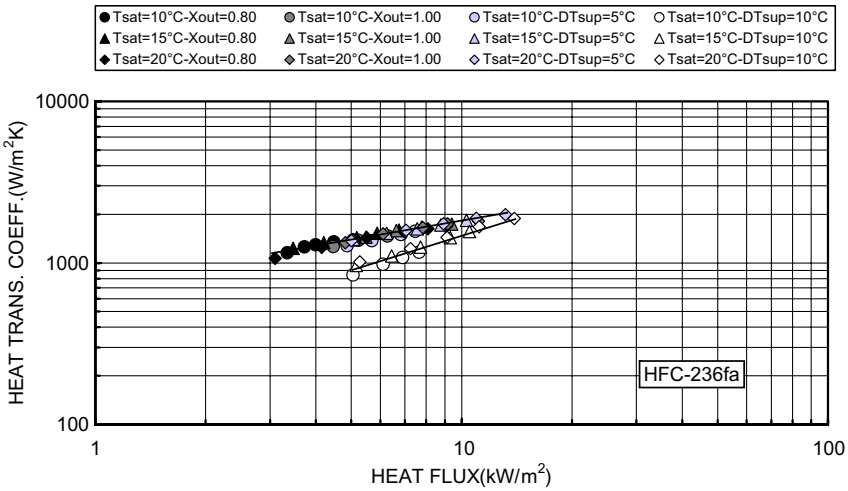

Fig. 4. Average heat transfer coefficient on refrigerant side vs. heat flux: HFC-236fa.

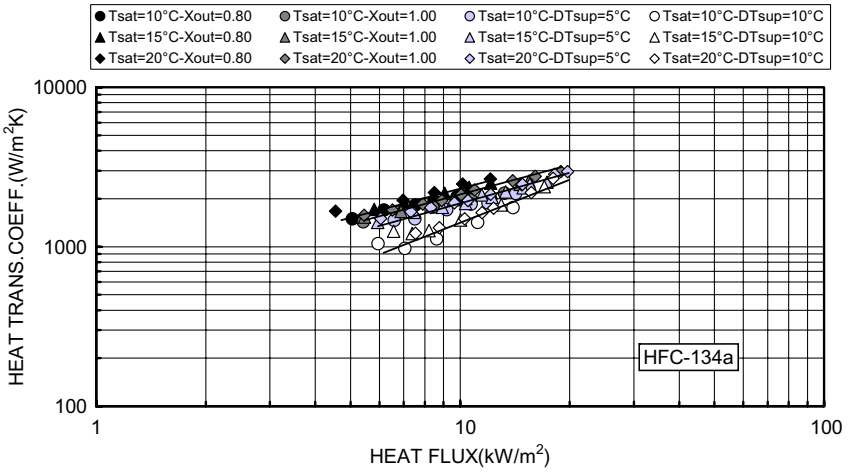

Fig. 5. Average heat transfer coefficient on refrigerant side vs. heat flux: HFC-134a.

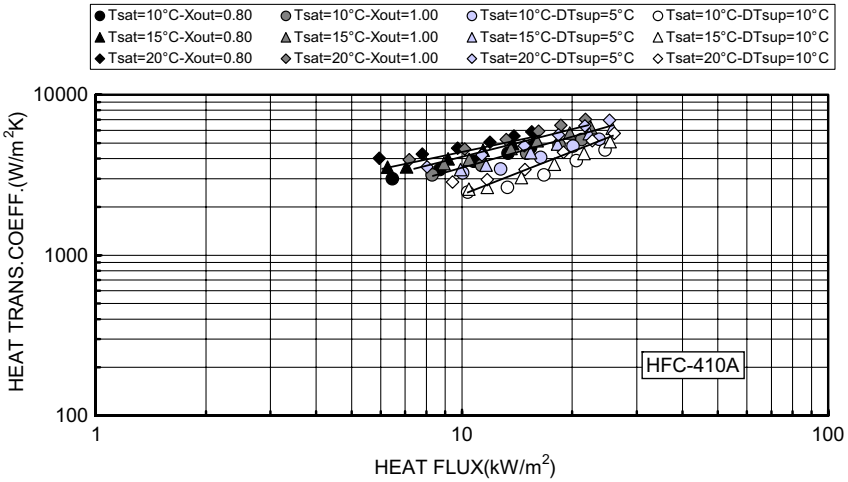

Fig. 6. Average heat transfer coefficient on refrigerant side vs. heat flux: HFC-410A.

transfer area of the evaporator defined in Eq. (3). Fig. 7 shows the comparison between saturated boiling experimental data and Cooper [19] equation: the mean absolute percentage deviations are 8.2%, 12.7% and 34.5% for HFC-134a, HFC-410A and HFC236fa data, respectively.

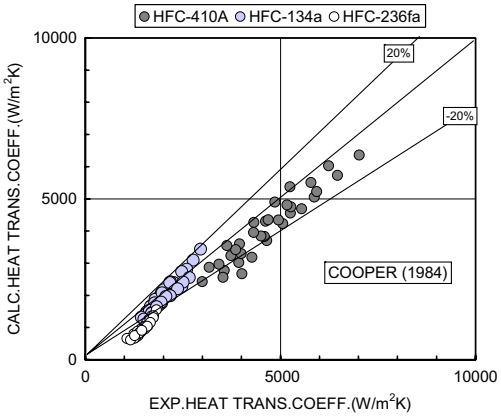

Fig. 7. Comparison between experimental and calculated saturated boiling heat transfer coefficient by Cooper [19] equation.

The Gorenflo [20] correlation is valid for pool boiling and accounts for heat flux, surface roughness and reduced pressure effects as follows:

$$h_r = h_0 C_{Ra} F(p^*)(q/q_0)^n \tag{26}$$

where

$$h_0 = 3500\ \mathrm{W/m^2\ K} \quad \text{(HFC-134a)} \tag{27}$$

$$h_0 = 4400\ \mathrm{W/m^2\ K} \quad \text{(HFC-410A)} \tag{28}$$

$$h_0 = 2850\ \mathrm{W/m^2\ K} \quad \text{(HFC-236fa)} \tag{29}$$

are the reference values ($p^*_0 = 0.1$, $q_0 = 20000\ \mathrm{W/m^2}$, $R_{a0} = 0.4\ \mu\mathrm{m}$) of the heat transfer coefficient for the three different HCF refrigerants;

$$C_{Ra} = (R_a/0.4\ \mu\mathrm{m})^{0.1333} \tag{30}$$

accounts for the effect of the arithmetic mean roughness R_a (μm) of the surface as defined in ISO4287/1;

$$F(p^*) = 1.2p^{*0.27} + [2.5 + 1/(1-p^*)]p^* \tag{31}$$

accounts for reduced pressure p^* effect;

$$(q/q_0)^n = (q/20000\ \mathrm{W/m^2})^{(0.9-0.3(p^*)\wedge 0.3)} \tag{32}$$

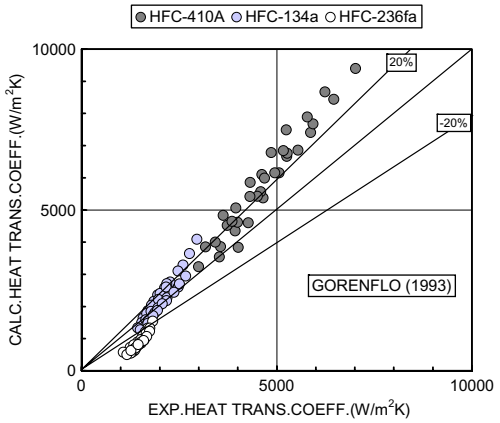

Fig. 8. Comparison between experimental and calculated saturated boiling heat transfer coefficient by Gorenflo [20] equation.

accounts for the heat flux q ($\mathrm{W/m^2}$) effect. In the present analysis the heat transfer coefficient and heat flux are referred to the nominal heat transfer area of the evaporator. Fig. 8 shows the comparison between saturated boiling experimental data and Gorenflo [20] equation: the mean absolute percentage deviations are 12.3%, 23.9% and 40.7% for HFC-134a, HFC-410A and HFC236fa data, respectively.

Cooper [19] and Gorenflo [20] correlations are able to reproduce HFC-134a and HFC-410A data, whereas both underpredict HFC-236fa data. This might be due to the fact that HFC-134a and HFC-410A saturated boiling data are controlled only by nucleate boiling, whereas HFC-236fa saturated boiling data is affected both by nucleate boiling and convective boiling. In order to verify this hypothesis present saturated boiling experimental data are compared against a quantitative criterion to determine the dominant heat transfer regime during vaporisation inside BPHE: the criterion by Thonon et al. [21]. This criterion is based on the Boiling number Bo and the Martinelli parameter X_{tt}

$$Bo = q/G\Delta J_{LG} \tag{33}$$

$$X_{tt} = [(1-X_m)/X_m]^{0.9}(\rho_G/\rho_L)^{0.5}(\mu_L/\mu_G)^{0.1} \tag{34}$$

$$BoX_{tt} > 0.15\times 10^{-3} \quad \Rightarrow \quad \text{Nucleate Boiling} \tag{35}$$

$$BoX_{tt} < 0.15\times 10^{-3} \quad \Rightarrow \quad \text{Convective Boiling} \tag{36}$$

where L and G refer to liquid and vapour phase, respectively.

Fig. 9 shows present saturated boiling experimental data on the map based on Thonon et al. [21] criterion: HFC-134a and HFC-410A data belong to the nucleate boiling zone, whereas HFC-236fa data approaches the boundary between nucleate boiling zone and convective boiling zone.

Fig. 10 shows the saturated boiling frictional pressure drop ($X_{out} \leqslant 1$) of HFC-134a, HFC-410A and HFC-236fa at different saturation temperatures (10, 15 and 20 °C) against the refrigerant mass flux: HFC-410A shows frictional pressure drops 40–50% lower than HFC-134a and 50–60% lower than HFC-236fa under the same mass flux.

Fig. 11 shows the saturated boiling frictional pressure drop ($X_{out} \leqslant 1$) of HFC-134a, HFC-410A and HFC-236fa against the kinetic energy of the refrigerant flow per unit volume

$$\mathrm{KE}/V = G^2/(2\rho_m) \tag{37}$$

computed by the homogeneous model. The frictional pressure drop shows a linear dependence on the kinetic energy per unit volume as already found by Jassim et al. [9] in adiabatic two-phase flow of HFC-134a through a PHE with herringbone and bumpy corrugation. It should be noted that in the present work the kinetic energy per unit volume of the two phase flow is computed by the homogeneous

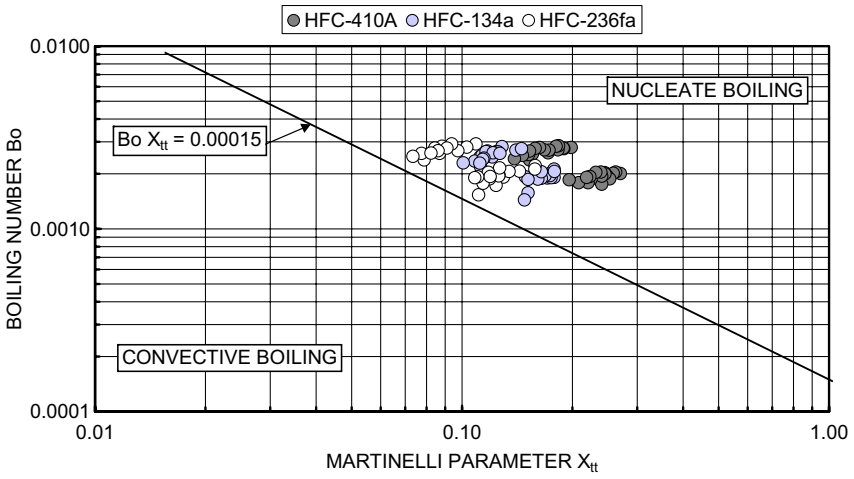

Fig. 9. Saturated boiling experimental data vs. Thonon et al. [21] criterion.

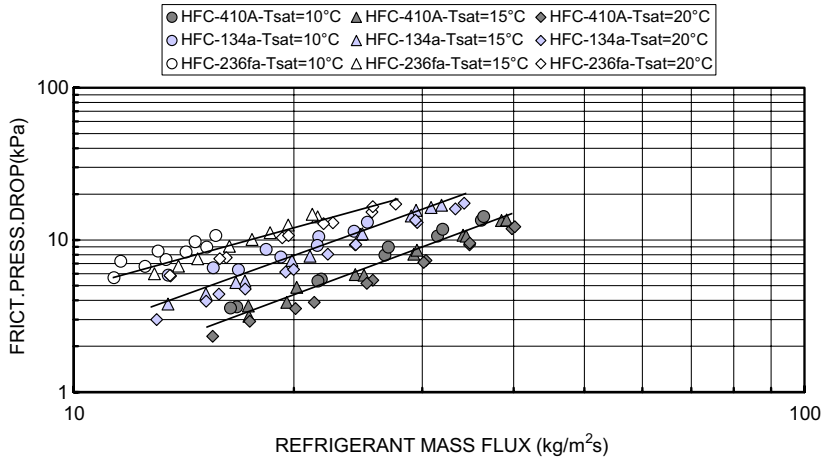

Fig. 10. Saturated boiling frictional pressure drop vs. refrigerant mass flux.

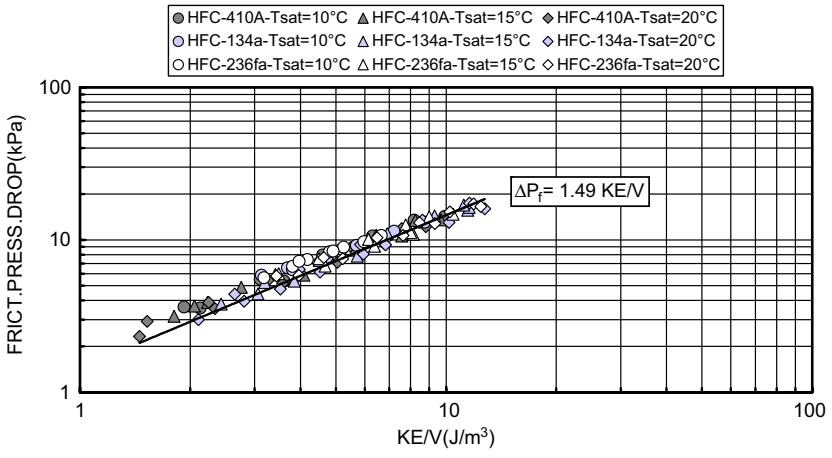

Fig. 11. Saturated boiling frictional pressure drop vs. kinetic energy per unit volume.

model, whereas Jassim et al. [9] have developed a specific void fraction model.

The following best fitting equation has been derived from the experimental data:

$$\Delta P_{\mathrm{f}} = 1.49\ \mathrm{KE/V} \tag{38}$$

This correlation reproduces present experimental data with a mean absolute percentage deviation around 8.8%.

It should be noted also that for the present sets of experimental data the frictional pressure drop ranges from the 91.0 to 99.4% of the total pressure drop measured.

5. Conclusions

This paper investigates the effect of heat flux, mass flux, saturation temperature, outlet conditions and fluids properties on heat transfer and pressure drop during HFC-134a, HFC-410A and HFC-236fa vaporisation inside a small brazed plate heat exchanger.

The heat transfer coefficients show weak sensitivity to saturation pressure and great sensitivity to heat flux, outlet conditions and fluid properties. The frictional pressure drop shows a linear dependence on the kinetic energy per unit volume of the refrigerant flow.

HFC-410A shows heat transfer coefficients 40–50% higher than HFC-134a and 50–60% higher than HFC-236fa together with frictional pressure drops 40–50% lower than HFC-134a and 50–60% lower than HFC-236fa. This can be attributed mainly to the higher reduced pressure (+53% and +77%), higher liquid thermal conductivity (+15% and +24%) and lower liquid dynamic viscosity (−36% and −57%) of HFC-410A with respect to HFC-134a and HFC-236fa.

Cooper [19] and Gorenflo [20] correlations are able to reproduce saturated boiling HFC-134a and HFC-410A heat transfer coefficients ($X_{out} \leqslant 1$), whereas they underpredict HFC-236fa data. This performance seems to confirm that nucleate boiling controls HFC-134a and HFC-410A vaporisation data, whereas HFC-236fa data is influenced also by convective boiling. This hypothesis is also confirmed through comparison with the Thonon et al. [21] criterion.

A linear equation based on the kinetic energy per unit volume of the refrigerant flow is proposed for the computation of frictional pressure drop: this correlation reproduces saturated boiling frictional pressure drop ($X_{out} \leqslant 1$) with a mean absolute percentage deviation around 8.8%.

References

[1] Y.Y. Yan, T.F. Lin, Evaporation heat transfer and pressure drop of refrigerant R134a in a plate heat exchanger, ASME J. Heat Transfer 121 (1999) 118–127.
[2] Y.Y. Yan, H.C. Lio, T.F. Lin, Condensation heat transfer and pressure drop of refrigerant R134a in a plate heat exchanger, Int. J. Heat Mass Transfer 42 (1999) 993–1006.
[3] Y.Y. Hsieh, T.F. Lin, Saturated flow boiling heat transfer and pressure drop of refrigerant R410A in a vertical plate heat exchanger, Int. J. Heat Mass Transfer 45 (2002) 1033–1044.
[4] Y.Y. Hsieh, T.F. Lin, Evaporation heat transfer and pressure drop of refrigerant R410A in a vertical plate heat exchanger, ASME J. Heat Transfer 125 (2003) 852–857.
[5] D.H. Han, K.J. Lee, Y.H. Kim, Experiments on the characteristics of evaporation of R410A in brazed plate heat exchangers with different geometric configurations, Appl. Therm. Eng. 23 (2003) 1209–1225.
[6] A. Jokar, S.J. Eckels, M.H. Hosni, T.P. Gielda, Condensation heat transfer and pressure drop of brazed plate heat exchangers using refrigerant R134a, J. Enhanced Heat Transfer 11 (2004) 161–182.
[7] A. Jokar, M.H. Hosni, S.J. Eckels, Dimensional analysis on the evaporation and condensation of refrigerant R-134a in minichannel plate heat exchanger, Appl. Therm. Eng. 26 (2006) 2287–2300.
[8] W.S. Kuo, Y.M. Lie, Y.Y. Hsieh, T.F. Lin, Condensation heat transfer and pressure drop of refrigerant R410A flow in a vertical plate heat exchanger, Int. J. Heat Mass Transfer 48 (2005) 5205–5220.
[9] E.W. Jassim, T.A. Newell, J.C. Chato, Refrigerant pressure drop in chevron and bumpy style flat plate heat exchangers, Exp. Therm. Fluid Sci. 30 (2006) 213–222.
[10] E.W. Jassim, T.A. Newell, J.C. Chato, Two-Phase flow visualisation in chevron and bumpy style flat plate heat exchangers, Heat Transfer Eng. 27 (2006) 20–27.
[11] R.K. Shah, W.W. Focke, Plate heat exchangers and their design theory, in: R.K. Shah, E.C. Subbarao, R.A. Mashelkar (Eds.), Heat Transfer Equipment Design, Hemisphere, Washington, 1988, pp. 227–254.
[12] J. Claesson, Correction of logarithmic mean temperature difference in a compact brazed plate evaporator assuming heat flux governed flow boiling heat transfer coefficient, Int. J. Refrige. 28 (2005) 573–578.
[13] T. Dutto, J.C. Blaise, T. Benedic, Performances of brazed plate heat exchanger set in heat pump, in: Proc. 18th Int. Cong. Refrigeration, Montreal, Canada, 1991, pp. 1284–1288.
[14] P. Fernando, B. Palm, P. Lundqvist, E. Granryd, Propane heat pump with low refrigerant charge: design and laboratory tests, Int. J. Refrige. 27 (2004) 761–773.
[15] A. Muley, R.M. Manglik, Experimental study of turbulent flow heat transfer and pressure drop in a plate heat exchanger with chevron plates, ASME J. Heat Transfer 121 (1999) 110–121.
[16] NIST, Refrigerant properties computer code, REFPROP 7.0., 2002.
[17] S.J. Kline, F.A. McClintock, Describing uncertainties in single-sample experiments, Mech. Eng. 75 (1953) 3–8.
[18] J. Claesson, B. Palm, Boiling mechanism in a small compact brazed plate heat exchanger (CBE) by using thermochromic liquid crystals (TLC), in: Proc. 20th Int. Cong. Refrigeration, Sydney, Australia, 1999, paper no. 1177.
[19] M.G. Cooper, Heat flows rates in saturated pool boiling – a wide ranging examination using reduced properties, Advanced in Heat Transfer, Academic Press, Orlando, Florida, 1984, pp. 157–239.
[20] D. Gorenflo, Pool boiling, in: E.U. Schlünder (Ed.), VDI Heat Atlas, Dusseldorf, Germany, 1993, Ha1-25.
[21] B. Thonon, R. Vidil, C. Marvillet, Recent research and developments in plate heat exchangers, J. Enhanced Heat Transfer 2 (1995) 149–155.